mimic continuous bulge formation as the end-product of interaction and merging, and a strong episode of bulge formation at $z_{for} > 3.5$. Both are consistent with the observed CIRB. The high-redshift, dust-enshrouded, star formation in model C results in a high level of the predicted background at wavelengths $\lambda > 400\,\mu m$.

Although none of the currently available optical data reflect the large differences between these models, which originate in the different fractions of heavily extinguished objects, the predicted infrared/submillimetre counts are more interesting, as shown in Fig. 2. Comparison of IRAS data with the no-evolution curve at 60 μm suggests some evolution. However, it seems that the 60-μm band does not strongly discriminate between the various models of evolution. In contrast, the upward deviation at 200 μm is due to the contribution of the redshifted 100-μm maximum of the infrared energy distribution. This redshifting of steep spectra counterbalances distance dimming and can make high-z objects easier to detect than low-z ones. Submillimetre observations are thus quite sensitive to the high-z history. The model also predicts that, at 200 μm, 10–100-mJy sources (contributing to 15% of the background) are located mostly at $z \sim 0.5$–2.5, whereas at 60 μm, and at the typical sensitivity level of IRAS surveys, the sources are indeed located mostly at very low z.

The detection of these sources would be a strong test for assessing the level of the 'optically dark' side of galaxy formation. The C160 filter of the ISOPHOT instrument on board ISO has an effective wavelength $\lambda_{eff} \approx 175\,\mu m$ for typical spectra of distant galaxies, and a 10 mJy r.m.s. noise fluctuation per 1.5 arcmin pixel is reachable after integration times longer than ~256 s per pixel. Thus a deep survey with this instrument seems to be feasible and is indeed scheduled. However, one might be concerned that small-scale cirrus fluctuations could hide the sources and the background fluctuations that they induce. A comparative analysis of the expected power spectra due to (1) cirrus fluctuations in regions of various H I column densities, (2) background fluctuations once sources above the confusion limit have been removed, and (3) the detector noise, shows that, in clean regions of the sky ($N_{HI} \leq 10^{20}$ atoms cm^{-2}), a survey with 10 mJy r.m.s. sensitivity should not only detect most sources above the low cirrus fluctuations but could also see background fluctuations in excess of the detector noise fluctuations, on scales of 3–10 arcmin (see Fig. 3). Because model C has 6.3×10^5 sources per sr with fluxes >30 mJy, a deep survey of a ~1,000 arcmin^2 field might begin to 'break' the CIRB into $\sim 50 \pm 7$ discrete sources, an order of magnitude more than is expected without evolution. This number is sufficient to test the high level of evolution and even to begin to disentangle the various models. If detected, the level of background fluctuations can also help to constrain the redshift distribution of the sources.

The tentative discovery of the CIRB is now supported by our new study in the cleanest regions of the sky, where the foreground Galactic components are essentially negligible. The conversion of the CIRB into its contributing sources by means of a semi-analytic model of galaxy formation leads to predictions of faint galaxy counts at infrared and submillimetre wavelengths. In contrast with the status of IRAS 60-μm counts, 175-μm counts with ISO should be able to detect the predicted strong evolution, and even disentangle various models consistent with the level of the CIRB. Moreover, small-scale cirrus fluctuations cannot hide the presence of the sources. Consequently, our knowledge of the optical/infrared luminosity budget at $z \sim 0.5$–2.5 should improve rapidly. We are about to start unveiling the optically dark side of galaxy formation. □

Received 15 May; accepted 2 October 1997.

1. Lilly, S. J., Tresse, L., Hammer, F., Crampton, D. & Le Fèvre, O. The Canada–France Redshift Survey. VI. Evolution of the galaxy luminosity function to $z \sim 1$. *Astrophys. J.* **455,** 108–124 (1995).
2. Williams, R. E. *et al.* The Hubble Deep Field: observations, data reduction, and galaxy photometry. *Astron. J.* **112,** 1335–1389 (1996).
3. Lilly, S. J., Le Fèvre, O., Hammer, F. & Crampton, D. The Canada–France Redshift Survey: the luminosity density and star formation history of the universe to $z \sim 1$. *Astrophys. J.* **460,** L1–L4 (1996).
4. Madau, P. *et al.* High redshift galaxies in the Hubble Deep Field. Color selection and star formation history to $z \sim 4$. *Mon. Not. R. Astron. Soc.* **283,** 1388–1404 (1996).
5. Puget, J. L. *et al.* Tentative detection of a cosmic far-infrared background with COBE. *Astron. Astrophys.* **308,** L5–L8 (1996).
6. Soifer, B. T. & Neugebauer, G. The properties of infrared galaxies in the local Universe. *Astron. J.* **101,** 354–361 (1991).
7. Hacking, P. & Houck, J. R. A very deep IRAS survey at $l = 97°$, $b = 30°$. *Astrophys. J. Suppl. Ser.* **63,** 311–333 (1987).
8. Ashby, M. L. N., Hacking, P. B., Houck, J. R., Soifer, B. T. & Weisstein, E. W. A massive $z = 0.088$ supercluster and tests of starburst galaxy evolution at the North Ecliptic Pole. *Astrophys. J.* **456,** 428–436 (1996).
9. Rowan-Robinson, M. *et al.* Observations of the Hubble Deep Field with the Infrared Space Observatory. V. Spectral energy distributions, starburst models and star formation history. *Mon. Not. R. Astron. Soc.* (in the press).
10. Reach, W. T. *et al.* Far-infrared spectral observations of the galaxy by COBE. *Astrophys. J.* **451,** 188–199 (1995).
11. Hartmann, D. & Burton, W. B. *An Atlas of Galactic Neutral Hydrogen Emission* (Cambridge Univ. Press, 1995).
12. Boulanger, F. *et al.* The dust/gas correlation at high Galactic latitude. *Astron. Astrophys.* **312,** 256–262 (1996).
13. Lacey, C. & Silk, J. Tidally triggered galaxy formation. I. Evolution of the galaxy luminosity function. *Astrophys. J.* **381,** 14–32 (1991).
14. Kauffmann, G. A. M., White, S. D. M. & Guiderdoni, B. The formation and evolution of galaxies within merging dark matter haloes. *Mon. Not. R. Astron. Soc.* **264,** 201–218 (1993).
15. Guiderdoni, B., Hivon, E., Bouchet, F. R. & Maffei, B. Semi-analytic modelling of galaxy evolution in the IR/submm range. *Mon. Not. R. Astron. Soc.* (in the press).
16. Blumenthal, G. R., Faber, S. M., Primack, J. R. & Rees, M. J. Formation of galaxies and large-scale structure with cold dark matter. *Nature* **311,** 517–525 (1984).
17. Heyl, J. S., Cole, S., Frenk, C. S. & Navarro, J. F. Galaxy formation in a variety of hierarchical models. *Mon. Not. R. Astron. Soc.* **274,** 755–768 (1995).
18. Kennicutt, R. C., Tamblyn, P. & Congdon, C. W. Past and future star formation in disk galaxies. *Astrophys. J.* **435,** 22–36 (1994).
19. Pascarelle, S. M., Windhorst, R. A., Keel, W. C. & Odewahn, S. C. Sub-galactic clumps at a redshift of 2.39 and implications for galaxy formation. *Nature* **383,** 45–50 (1996).
20. Zepf, S. E. & Koo, D. C. Close pairs of galaxies in deep sky surveys. *Astrophys. J.* **337,** 34–44 (1989).
21. Burkey, J. M., Keel, W. C., Windhorst, R. A. & Franklin, B. E. Galaxy pairs in deep HST images: evidence for evolution in the galaxy merger rate. *Astrophys. J.* **429,** L13–L17 (1994).
22. Carlberg, R. G., Pritchet. C. J. & Infante, L. A survey of faint galaxy pairs. *Astrophys. J.* **435,** 540–547 (1994).
23. Sanders, D. B. & Mirabel, I. F. Luminous infrared galaxies. *Annu. Rev. Astron. Astrophys.* **34,** 749–792 (1996).
24. Soifer, B. T. *et al.* The IRAS Bright Galaxy Sample. II. The sample and luminosity function. *Astrophys. J.* **320,** 238–257 (1987).
25. Hauser, M. G. in *Unveiling the Cosmic Infrared Background* (ed. Dwek, E.) 11–21 (AIP Conf. Proc. 348, 1996).
26. Lonsdale, C. J., Hacking, P. B., Conrow, T. P. & Rowan-Robinson, M. Galaxy evolution and large-scale structure in the far-infrared. II. The IRAS faint source survey. *Astrophys. J.* **358,** 60–80 (1990).
27. Rowan-Robinson, M., Saunders, W., Lawrence, A. & Leech, K. The QMW IRAS galaxy catalogue: a highly complete and reliable IRAS 60-μm galaxy catalogue. *Mon. Not. R. Astron. Soc.* **253,** 485–495 (1991).
28. Bertin, E., Dennefeld, M. & Moshir, M. Galaxy evolution at low redshift? II. Number counts and optical identifications of faint IRAS sources. *Astron. Astrophys.* **323,** 685–696 (1997).
29. Gautier, T. N. III, Boulanger, F., Perault, M. & Puget, J. L. A calculation of confusion noise due to infrared cirrus. *Astron. J.* **103,** 1313–1324 (1992).

Acknowledgements. We thank Dave Clements, François-Xavier Désert and Bruno Maffei for their comments and suggestions.

Correspondence and requests for materials should be addressed to B.G. (e-mail: guider@iap.fr).

Phase transitions in individual sub-micrometre superconductors

A. K. Geim, I. V. Grigorieva, S. V. Dubonos*, J. G. S. Lok, J. C. Maan, A. E. Filippov† & F. M. Peeters‡

Research Institute for Materials, University of Nijmegen, 6525 ED Nijmegen, The Netherlands

** Institute for Microelectronics Technology of RAS, 142432 Chernogolovka, Russia*

† Physical-Technical Institute of NASU, 340114 Donetsk, Ukraine

‡ Department of Physics, University of Antwerp (UIA), B-2610 Antwerp, Belgium

The properties of a superconductor are expected to change radically when its size becomes comparable to that of the Cooper pairs, the quasiparticles responsible for superconductivity. The effect of such confinement is well understood for the case of the suppression of superconductivity by magnetic fields (which gives rise to so-called Little–Parks oscillations of the phase boundary)[1–4]. But little is known about what happens in small superconductors in the zero-resistance state, which cannot be

probed by resistance measurements. Here we apply a new technique of ballistic Hall magnetometry[5] to study the magnetization of individual superconducting discs of diameters down to 100 nm. The superconducting state of these discs is found to be qualitatively different from both macroscopic and microscopic[6] superconductors, with numerous phase transitions whose character changes rapidly with size and temperature. This exotic behaviour is due to size quantization of the Cooper-pair motion and resulting transitions between discrete states of the superconducting Bose condensate in a magnetic field.

The oscillating superconducting phase boundary of small hollow cylinders[2] and discs [3,4] (the Little–Parks effect) implies that spatial confinement should also essentially change the superconducting state of samples whose size is comparable to the characteristic size of Cooper pairs (coherence length ξ)[1] and the superconductivity of which is destroyed by only a few magnetic flux quanta. Although the Little–Parks effect has been known for almost 40 years, it has so far proved to be impossible to conduct analogous studies inside the superconducting state, mainly because the commonly used resistance measurements are unsuitable as the resistance remains zero even if there are changes occurring below the superconducting transition temperature (T_C). A technique recently developed by our group and referred to as ballistic Hall micro-magnetometry[5] allows us to perform thermodynamic studies of individual superconducting grains and thus to probe their superconducting state below T_C. The technique enables the detection of magnetization changes of $\sim 10^3$ Bohr magnetons ($\sim 10^{-17}$ emu) and its details are briefly described in the legend to Fig. 1. The smallest sample from which we were able to get a reliable superconducting response was only $\sim$100 nm in size and even this limit is mainly due to the absence of the Meissner effect in such small particles[1,6].

Figure 2 shows several magnetization curves that demonstrate a surprising diversity of behaviour in mesoscopic superconductors: a change of only a factor of two in the size of sub-micrometre aluminium discs drastically changes their superconducting response. The smallest sample of Fig. 2a and smaller discs exhibit a simple magnetization response, with the second-order phase transition between the normal and superconducting states (smooth decay of magnetization). Such behaviour is the same as that expected for thin films in parallel field and is in agreement with theory[1]. For the sample of twice the size, the superconducting phase transition unexpectedly becomes first order (as indicated by a jump in magnetization) and is accompanied by a well-defined bistable region where the sample can be either superconducting or normal, depending on the direction of the magnetic sweep. Both states can live for several hours (so it was not possible to determine which one was thermodynamically stable) and were found only for a very narrow range of sizes ($r \approx \xi(0)$) and at temperatures far below T_C. When the sample size was increased further, we found that the superconducting phase transition became second order again. In addition, numerous magnetization jumps appeared, indicating first-order phase transitions inside the superconducting state. Although the magnetization $M(H)$ depends on the direction of the field sweep, the remanent magnetization always remains zero, indicating the absence of detectable bulk pinning. The hysteresis in $M(H)$ is due to the surface (Bean–Livingston) barrier.

The initial stages of magnetization of the large discs (Fig. 2c, d) can be understood qualitatively as an entry or exit of individual vortices into or out of the superconductor. Indeed, although the height of the magnetization jumps here is not quantized, they are all of about one flux quantum, ϕ_0. However, in higher fields and for the

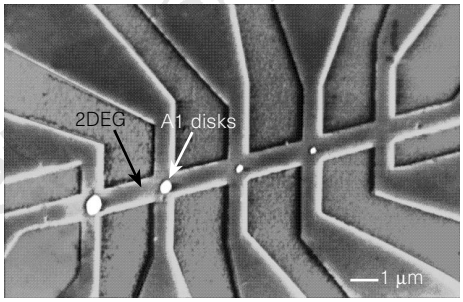

Figure 1 Scanning electron micrograph (viewed at an angle) of our experimental devices. It shows five Hall probes made from GaAlAs/GaAs heterostructures with a two-dimensional electron gas (2DEG) embedded 60 nm below the surface. Superconducting Al discs of various diameters are deposited in the probes' sensitive areas and electrically insulated from the 2DEG. Ballistic Hall magnetometry is based on precise measurements of the magnetic field in the direct vicinity of a mesoscopic sample placed in the central area of a sub-micrometre Hall probe. Owing to a relatively low electron concentration, a 2DEG provides large, easily measurable Hall response. However, the main reason for using a 2DEG is that electrons move ballistically inside the cross junction. For ballistic motion, the Hall voltage is simply given by the average magnetic field in the cross junction, that is, $R_{xy} \propto \langle B \rangle / ne$, thus allowing straightforward quantitative analysis. Because the magnetic flux inside the cross junction is $\Phi = \langle B \rangle S$, these ballistic Hall probes are in fact micro-fluxmeters, similar to SQUIDs but with an effective detection loop of only $\sim 1\ \mu m^2$. The difference between the Hall signal for the probes with and without a superconducting sample gives directly the magnetization $4\pi M = \langle B \rangle - H$.

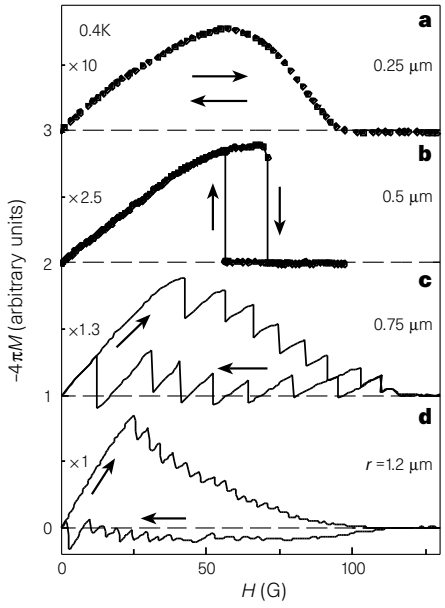

Figure 2 Magnetization responses of individual sub-micrometre Al discs of various radii. Radii are 0.25 (**a**), 0.50 (**b**), 0.75 (**c**) and 1.20 μm (**d**). The curves are reproducible within the line width, even after thermal cycling to room temperature. Arrows show the direction of the magnetic field sweep. Aluminium is a favourable material for studies of mesoscopic superconductivity owing to its large coherence length $\xi(T = 0\,K)$, which can be of the order of 1 μm even in evaporated thin films with typically short electron mean free path l. The resistivity of our macroscopic Al films yields an l of ~50 nm, varying by a factor of 2 depending on the film thickness and evaporation conditions. T_C is ~1.3 K. This allows us to estimate the superconducting parameters[1]: $\xi(0\,K) \approx 250$ nm and $\lambda(0) \approx 70$ nm; that is, in the bulk our material is a type-I superconductor. We have measured the magnetization of many discs with radii r of 70 nm to 1.3 μm and heights of 70 nm to 0.15 μm. The curves presented are for height 0.13 μm, but no qualitative difference in the behaviour is found for the other heights.

largest samples (as in Fig. 2d) the flux jumps become only a small fraction of ϕ_0 and eventually disappear in the noise. This observation is in striking contrast with the common belief that the field penetrates in superconductors in units of ϕ_0. There are also several other peculiar features on the magnetization curves (for example, smooth penetration of magnetic field between flux jumps) that will be discussed elsewhere.

The drastic changes in the superconducting response with changes in sample size can be understood qualitatively as entering three different regimes with respect to the size of Cooper pairs: $r \leqslant \xi$ (upper curve), $r \approx \xi$ (middle) and $r > \xi$ (two lower curves). Alternatively, $r \approx \xi$ implies $H_{c2}S/\phi_0 \approx 1$, where $H_{c2} = \phi_0/2\pi\xi^2$ is the critical field[1], and our mesoscopic superconductors can also be described as 'few-flux-quanta' superconductors in which the superconductivity is destroyed by only a few vortices. The parameter that is expected to determine the observed behaviour is the relative size of the sample, r/ξ. Indeed, because $\xi(T) \approx \xi(0)[1 - (T/T_C)]^{-1/2}$ (ref. 1), we could move between the various regimes by varying the temperature, for example the disc with $r = 0.5\,\mu$m at $T < 0.8$ K exhibits an $M(H)$ similar to that for the 0.25 μm disc at 0.4 K. Although for most experimental features there is good scaling between different temperatures and sizes, the bistable region was never observed above 0.8 K.

To understand the unexpected bistable superconductivity, we have measured the superconducting phase boundary for several samples in the regime $r \approx \xi(0)$. Figure 3 shows $H_{cr}(T)$ for the 'two-flux-quanta' superconductor and, for comparison, $H_{cr}(T)$ of a macroscopic aluminium film deposited simultaneously with the disc. All the difference between the two diagrams stems from the presence of the sample boundary. The diagram for the small disc exhibits an arc-type behaviour that at temperatures close to T_C is known as Little–Parks oscillations (at lower temperatures these oscillations were previously not accessible)[2–4]. We find that the arcs continue into lower temperatures where the bistable region appears as a splitting into two branches that starts at precisely the same temperature as that at which the superconducting transition changes its order.

For a quantitative analysis of the observed phase diagrams, we use the linearized Ginzburg–Landau (GL) equation[1–4]. As demonstrated in Fig. 3, it describes the phase diagram of the mesoscopic disc perfectly, with no fitting parameters (ξ is determined experimentally from the reference film). The different arcs in Fig. 3 correspond to quantum states (solutions of the GL equation) with different orbital momenta L. They describe different distributions of the superconducting current in the disc and can be viewed as giant multi-quanta vortices[4] (Fig. 3, insets). The overall increase in H_{cr} in the mesoscopic sample relative to the film is by a factor of ~1.7 and is obviously related to the surface superconductivity ($H_{c3} = 1.69H_{c2}$) (ref. 1).

Surprisingly, the curves in Fig. 3 describe the phase boundary accurately even at low T, although GL equations are generally no longer valid in this temperature interval[1]. The theoretical fit imparts a very clear physical meaning to the bistable region in Fig. 3: the latter corresponds to the transition between the ground ($L = 2$) and first excited ($L = 1$) states of the superconducting condensate. The quantized bistability is bound to low temperatures but not to any particular value of L, because for other samples (with slightly different r/ξ) it has also been observed for transitions between $L = 0$ and 1 and between $L = 2$ and 3. The bistability suggests the presence of a potential barrier between different L states, whereas its absence at temperatures close to T_C probably indicates that it is destroyed by thermal activation above the barrier.

Now we turn to the discussion of the transitions observed inside the superconducting state of larger discs (Fig. 2c). The magnetization jumps unambiguously indicate first-order phase transitions between discrete thermodynamic states of the superconducting

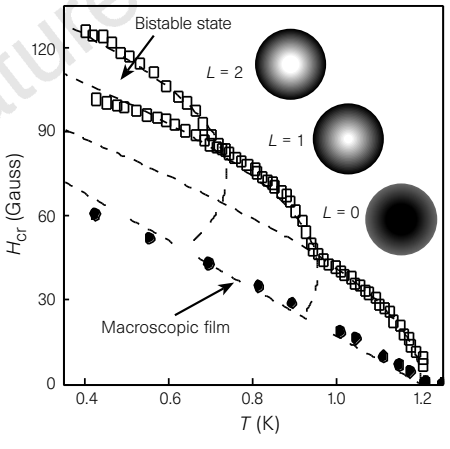

Figure 3 Typical superconducting phase diagram observed for mesoscopic disks with $r \approx \xi(0)$. The critical field H_{cr} is measured as the onset of the magnetization response at different temperatures. The squares show the diagram for a 0.55-μm Al disc (thickness 0.08 μm); the ovals are for the reference Al film. The broken curves show the corresponding solutions of the linearized GL equation. For the macroscopic film, the equation yields the known expression $H_{cr}(T) = \phi_0/2\pi\xi(T)^2 = \phi_0/2\pi\xi(0)(1 - T/T_C)$ (ref. 1), which describes the experimental temperature dependence well. The fit yields $\xi(0) \approx 0.2\,\mu$m, in agreement with the value found independently from the film resistivity. The calculated distribution of the order parameter for different states L is shown as insets: black corresponds to the maximum of the order parameter, and white to its minimum.

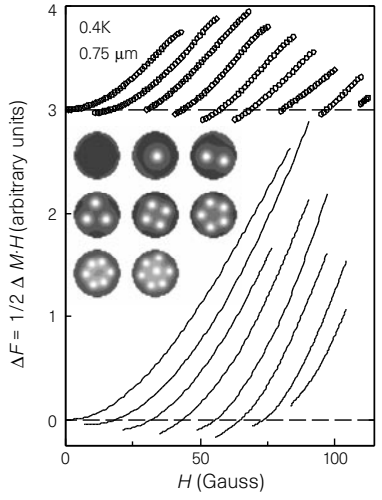

Figure 4 Energy of the superconducting states observed in the 0.75 μm disc of Fig. 2 plotted against magnetic field at 0.4 K (top). The magnetization data are converted into energy by using the equation $\Delta F = M^*H/2$. The data were obtained by sweeping the magnetic field up and down, starting at different fields, so that all possible states of the mesoscopic system could be scanned. The superconductor can evolve along any of the curves until it becomes unstable and switches to the next state either by the entry or the exit of a vortex. The stability range is defined by the surface barrier. Switch-overs between different states (jumps in the magnetization) are omitted from the plot. The lower part of the figure shows numerical simulation of our experiment with the full set of two-dimensional GL equations. The large range of stability on the theoretical curves is due to the cylindrical geometry used in the simulations, which ignores demagnetization effects.

condensate. The dependence of the energy of these states on the magnetic field is plotted in Fig. 4 (top). One could predict that such states are due to different numbers of Abrikosov vortices that can fit into a small volume. The situation resembles magnetization peaks observed in layered superconductors as the result of varying numbers of vortex rows in the sample[7,8]. The initial stages of magnetization in mesoscopic superconductors were also described as evolution along different vortex phases in recent theoretical works, using a semi-classical model of interacting vortices[9,10]. We have obtained a better and more complete description of the experimental data by numerically solving the nonlinear GL equations[1,8]; the results are shown in Fig. 4. The quantum states clearly correspond to integral numbers N of Abrikosov vortices (Fig. 4, insets). The different curves $\Delta F(H)$ are shifted along the horizontal axis by $\Delta H \approx \phi_0/s$, indicating one-by-one entries of vortex cores inside the disk area s. Note that although the number of vortices in the sample is quantized, there is no quantization of the magnetic flux because some of it 'spills out' of the sample owing to the presence of the boundary. This also leads to smooth penetration of the magnetic field inside the superconductor (nonlinear Meissner effect), which can be seen as the rounding of the upper parts of the curves in Figs 2 and 4.

Although the presence of the sample boundary explains the non-quantized flux jumps qualitatively, neither of the existing theories predicts the possibility of fractional jumps (much smaller than ϕ_0) observed in our largest, multi-flux-quanta superconductors in high fields. We attribute them to changes in the vortex configurations for a constant number of vortices inside the superconductor. Indeed, our numerical simulations of the GL equations find multiple stable vortex configurations for $N \geqslant 5$ (vortex configurations are also discussed in refs 8, 10). Different configurations assume different energies and lead to different amounts of magnetic flux spilling out. Therefore, transitions between such states occur with minor flux jumps. The number of possible vortex configurations increases with increasing N, which can explain the jumps getting smaller with increasing field. It is also possible that shape irregularities allow additional vortex configurations.

Finally, there is a clear analogy between our work and current intensive studies of electron spectra in confined geometries, commonly referred to as quantum dots or artificial atoms (reviewed in ref. 11). In fact, the GL equations can be seen physically as a Schrödinger-type equation for the centre-of-mass motion of Cooper pairs (with strong non-local interaction via vector potential)[1]. From this viewpoint, mesoscopic superconductors present "artificial atoms made from Cooper pairs rather than electrons" and we can equally interpret Figs 3 and 4 in terms of energy spectra of non-interacting and interacting Cooper pairs, respectively. □

Received 8 May; accepted 23 September 1997.

1. de Gennes, P. G. *Superconductivity in Metals and Alloys* (Addison-Wesley, New York, 1989).
2. Parks, R. D. & Little, W. A. Fluxoid quantization in a multiply-connected superconductor. *Phys. Rev.* A **133,** 97–103 (1964).
3. Buisson, O., Gandit, P., Rammal, R., Wang, Y. Y. & Pannetier, B. Magnetization oscillations of a superconducting disk. *Phys. Lett.* A **150,** 36–42 (1990).
4. Moshchalkov, V. V. *et al.* Effect of sample topology on the critical fields of mesoscopic superconductors. *Nature* **373,** 319–322 (1995).
5. Geim, A. K. *et al.* Ballistic Hall micromagnetometry. *Appl. Phys. Lett.* **71,** 2379–2381 (1997).
6. Black, C. T., Ralph, D. C. & Tinkham, M. Spectroscopy of the superconducting gap in individual nanometer-scale aluminum particles. *Phys. Rev. Lett.* **76,** 688–691 (1996).
7. Brongersma, S. H., Verweij, E., Koeman, N. J., de Groot, D. G. & Griessen, R. Series of maxima in the field dependent magnetic moment of layered superconductors. *Phys. Rev. Lett.* **71,** 2319–2322 (1993).
8. Bolech, A. C., Buscaglia, G. C. & Lopez, A. Numerical simulation of vortex arrays in thin superconducting films. *Phys. Rev.* B **52,** 15719–15722 (1995).
9. Buzdin, A. I. & Brison, J. P. Vortex structures in small superconducting disks. *Phys. Lett.* A **196,** 267–271 (1994).
10. Krasilnikov, A. S., Mamsurova, L. G., Trusevich, N. G., Shcherbakova, L. G. & Pukhov, K. K. Fine-grained YBaCuO: the formation of the initial vortex lattice and the magnetization curves. *Supercond. Sci. Technol.* **8,** 1–5 (1995).
11. Ashoori, R. C. Electrons in artificial atoms. *Nature* **379,** 413–419 (1996).

Acknowledgements. We thank INTAS, FOM and NATO for financial support.

Correspondence and requests for materials should be addressed to A.K.G. (e-mail: geim@sci.kun.nl).

Giant fluctuations in a free diffusion process

Alberto Vailati & Marzio Giglio

Dipartimento di Fisica and Istituto Nazionale per la Fisica della Materia, Università di Milano, via Celoria 16, 20133 Milano, Italy

Macroscopic concentration gradients in physical systems relax towards equilibrium by diffusion[1–3], in the absence of bulk motion. This is normally regarded as a spatially homogeneous mixing process. Here, however, we show that unexpectedly large spatial fluctuations in concentration can occur during a free diffusion process. We set up an initially sharp interface between two miscible fluids by letting a mixture phase-separate below the critical consolution temperature and then raising the temperature quickly to the single-phase region. Shadowgraph images and low-angle light scattering show evidence for large fluctuations in composition, orders of magnitude larger in amplitude than those seen in the equilibrium state. We show that these pronounced inhomogeneities are due to a coupling between velocity

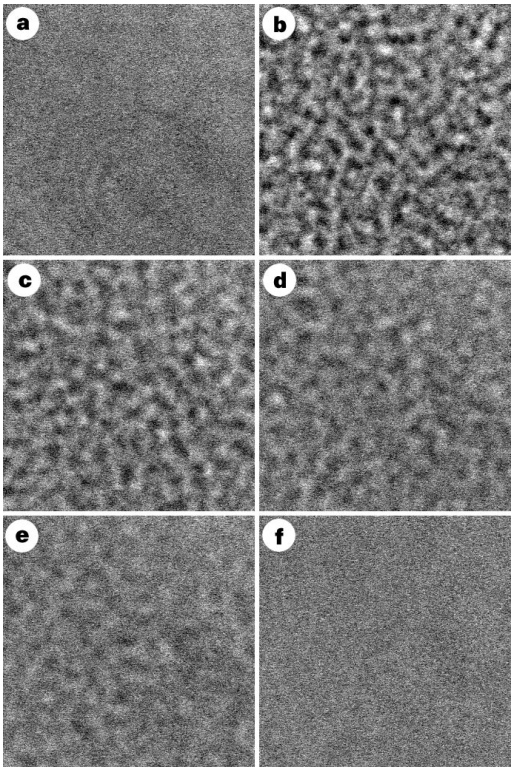

Figure 1 Shadowgraph images of the sample during the diffusion process. The images were generated by shining a vertical white-light beam on an horizontal layer of sample and by imaging the sample slightly out of focus on a CCD (charge-coupled device) camera. Image **a** was acquired when the sample was kept below its critical temperature T_c, where the sample consists of two layers of immiscible fluids separated by a sharp interface, and no diffusion occurs. A temperature jump was then applied to bring the sample above T_c, where the two layers become miscible, and the diffusion process started. The images **b–f** were taken at different times after the application of the temperature jump: **b**. 100 s; **c**, 9 min; **d**, 90 min; **e**, 330 min; and **f**, 3 days. To get rid of non-uniform illumination, the images were processed by subtracting a reference image acquired when the sample was homogeneous. The side of each image is 1 mm in real space.